Chinese Journal of Chemical Engineering 85 (2025) 348–354

Contents lists available at ScienceDirect

Chinese Journal of Chemical Engineering

journal homepage: www.elsevier.com/locate/CJChE

Full Length Article

Modulating titanium dioxide electron transport layer by self-doping for high-efficiency carbon-based perovskite solar cells

Xin Peng , Rong Huang , Wenran Wang *, Jianxin Zhang , Zhenxiao Pan , Yueping Fang , Huashang Rao , Xinhua Zhong *, Guizhi Zhang *

Key Laboratory for Biobased Materials and Energy of Ministry of Education, College of Materials and Energy, South China Agricultural University, Guangzhou 510642, China

ARTICLE INFO

Article history:
Received 9 December 2024
Received in revised form
22 February 2025
Accepted 5 March 2025
Available online 1 July 2025

Keywords:
Perovskite
Solar cell
$CsPbI_3$
Carbon electrode
Electron transport layer

ABSTRACT

In perovskite solar cells (PSCs), it is important to construct electron transport layer (ETL) with ideal surface morphology and advantageous electron transport dynamics. In this work, a functional TiO_2 ETL is designed and constructed based on a novel Ti^{3+} self-doping strategy. Experimental results indicate that Ti^{3+} dopant can optimize TiO_2 film crystallization process by facilitating the assembly of precursor particles, reducing the content of pore-forming reagent, and enhancing the adhesion of precursors to glass substrate in film formation process. Therefore, the modified surface morphology inhibits the formation of undesired hole structure. Besides, self-doping moderately generates oxygen vacancies on TiO_2 surface and a shallower TiO_2 Fermi energy level. These not only result in a stronger interfacial electronic coupling, but also establish an advantageous energy band alignment. These merits optimize interfacial electron transfer dynamics by inhibiting recombination loss and facilitating electron extraction. Benefiting from the optimized TiO_2 ETL, hole transport layer (HTL)-free carbon electrode based $CsPbI_3$ PSCs deliver a high efficiency of 18.62%, representing one of the highest levels in this field.

1. Introduction

Perovskite solar cells (PSCs) represent one of the most attractive next-generation photovoltaic technologies with the outstanding high power conversion efficiency (PCE) beyond 26% [1–3]. Among them, hole transport layer (HTL)-free carbon electrode-based PSCs (C-PSCs) show the promising advantages of facile fabrication, high stability, and low cost [4–6]. Since there is no HTL in C-PSCs, the sole electron transport layer (ETL) plays the vital roles of extracting electrons and blocking holes. Therefore, the modulation of ETL properties, such as surface morphology, band structure, electron mobility, and defect state density, etc., is important for high-efficiency C-PSCs.

In terms of surface morphology, an ideal ETL requires high coverage and less holes, so that direct contact of perovskite to conductive substrate and undesired current leakage can be prevented. As for photovoltaic performance, it demands an optimal electron extraction and collection kinetics to prevent undesired charge recombination loss [7,8]. TiO_2 is a mainstream ETL material with a high annealing temperature (around 500 °C) [9]. This makes it adapt to high-efficiency inorganic perovskite systems with high crystallization temperatures [10–19]. However, there remains issues in conventional TiO_2 ETLs. TiO_2 ETLs are usually fabricated by solution-based methods such as sol-gel, spray coating, *etc.* The pore-forming behavior in annealing process and the lack of sufficiently strong interactions among titanium precursors result in the formation of TiO_2 layer with hole structures [20,21]. These can induce the direct contact of perovskite to conductive substrate, and undesired current leakage occurs. As for interfacial electron transfer dynamics, it requires ideal electronic coupling between bilateral materials. From the viewpoint of semiconductor energy band constitution, titanium cations contribute conduction band of TiO_2, so Ti cations can serve as the electron acceptors in charge transfer process [22]. Unfortunately, TiO_2 fabricated in ambient atmosphere exhibits an oxygen-rich surface, and the oxygen anions with large electronegativity acts as the barrier that hinders interfacial electron transfer [23,24]. If surface oxygen can be moderately removed, the exposed surface titanium cations are expected to facilitate electron extraction. Besides, band alignment

* Corresponding authors.
E-mail addresses: wwrwangwenran@scau.edu.cn (W. Wang), zhongxh@scau.edu.cn (X. Zhong), guizhi_zhang@scau.edu.cn (G. Zhang).

https://doi.org/10.1016/j.cjche.2025.03.022
1004-9541/© 2025

is another factor determining interfacial electron transport dynamics. For perovskite with a relatively shallow Fermi energy level (E_F), when it forms a heterojunction with TiO_2 with a deeper E_F, the conduction band of perovskite will bend upward and form an interfacial electron extraction barrier. Note that the barrier height is theoretically dictated by the E_F difference between perovskite and TiO_2 [25]. If a shallower Fermi level of TiO_2 can be realized, then the barrier height can be expected to reduce, thus enhancing built-in electric field and facilitating electron extraction [26]. In order to improve interfacial carrier dynamics, it is essential to manipulate TiO_2 crystallization and inhibit the formation of holes, as well as construct a moderate oxygen-deficient surface and optimize band alignment.

Doping of TiO_2 by introducing foreign atoms in titanium precursors can achieve these goals simultaneously. Suitable dopants, such as Mg^{2+} [27], Zn^{2+} [28], Sn^{2+} [29], Y^{3+} [30], Nb^{5+} [31], N [32], etc., can modulate TiO_2 crystallization kinetics, optimize TiO_2 morphology and surface chemistry. Besides, dopants in TiO_2 lattice can modulate electronic structures, and heavier n-type doping can result in a shallower E_F [32,33]. However, dopants with different radii and valences serve as deep extrinsic defects that induce charge recombination [34]. Compared with heteroatom dopants, self-doping by Ti^{3+} is a mild strategy [35,36]. This is because intrinsic n-type TiO_2 can thermally activate Ti^{3+},and self-doping does not induce heteroatoms or related deep energy levels. Since +4 is the thermodynamically stable valence state of Ti, even if abundant Ti^{3+} cations present in precursors, they can be mostly oxidized in annealing process in ambient atmosphere. As a result, the stoichiometric ratio of Ti/O in resultant TiO_2 deviates very limitedly, and the outstanding semiconductor properties of TiO_2 still preserve [35]. Besides, due to charge-compensating characteristic, the introduction of Ti^{3+} is accompanied by the formation of bulk and surface oxygen vacancies [22,37,38]. This is advantageous for the construction of an oxygen-deficient surface.

In this work, a functional TiO_2 ETL was designed and constructed by a novel self-doping strategy, in which Ti^{3+} as the dopant was introduced in conventional Ti(IV) sol solutions. It is found that the application of Ti^{3+} reduces the necessary content of bulky surfactant-containing precursors, which are undesired pyrolytic pore producers. Besides, Ti^{3+} promotes the assembly of titanium sol particles to enhance film compactness. Therefore, the morphology of TiO_2 ETL can be improved with less holes. As for material physics, self-doping results in the moderate formation of surface oxygen vacancies and exposed surface Ti cations. They can serve as electron trapping states and facilitate interfacial electron extraction according to theoretical calculation. In addition, self-doping enhances the electron density of TiO_2 and results in a shallower Fermi level. As a result, electron extraction barrier at perovskite/TiO_2 heterojunction interface is reduced. Benefiting from improved surface morphology and enhanced electron extraction dynamics of TiO_2 ETL, the optimal $CsPbI_3$ C-PSC exhibited a high PCE of 18.62% (V_{oc} = 1.132 V, J_{sc} = 19.84 mA·cm^{-2}, FF = 82.92%). To the best of our knowledge, this represents one of the highest levels in the field of inorganic C-PSCs [39–43].

2. Results and Discussion

2.1. Construction of compact TiO_2 ETL with less holes

Sol-gel is a common method in the construction of compact TiO_2 ETL. In this method, a sol solution containing titanium precursors (such as titanium diisopropoxide bis(acetylacetonate) (Ti(acac)$_2$(OiPr)$_2$), Fig. 1(a)) is spin coated on FTO substrate. Subsequently, sols condense to form a gel film, followed by pyrolysis at elevated temperature to form a TiO_2 film [44,45]. However, this method shows drawbacks. First, titanium-containing sol particles are capped by surfactants such as acetylacetone in our case. These molecules provide interparticle repulsion, which is

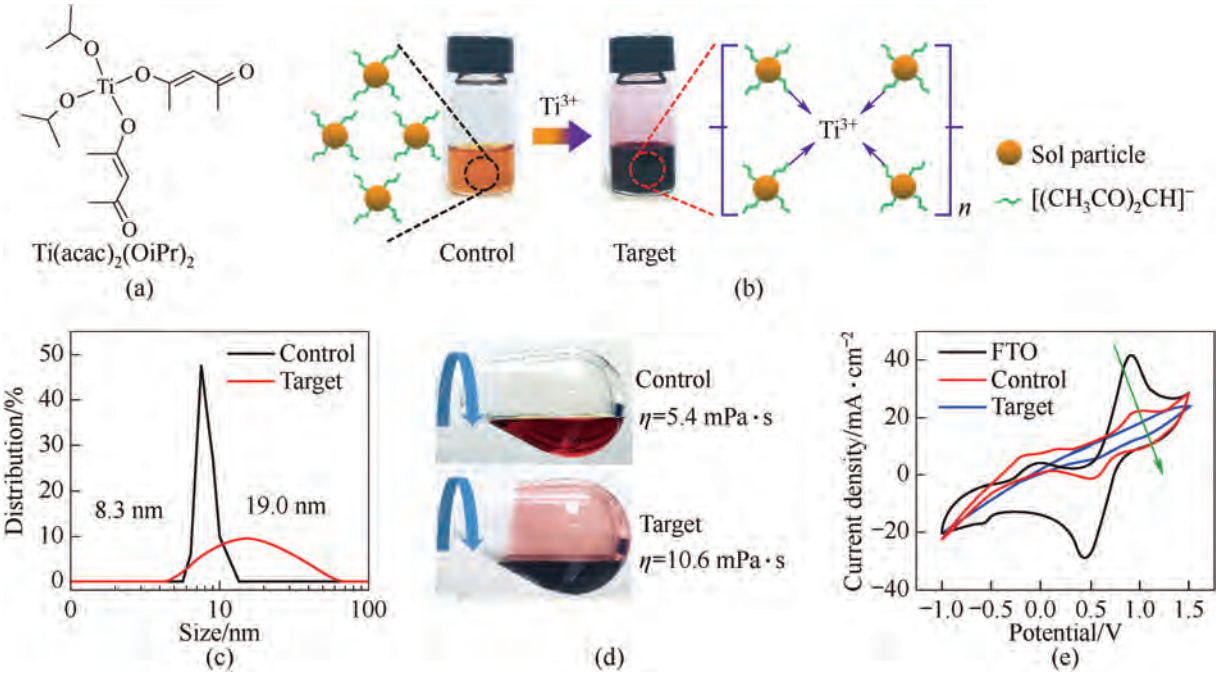

Fig. 1. (a) Molecular structure of Ti (acac)$_2$(OiPr)$_2$. (b) Photographs of control and target sol solutions and the schematic mechanism showing the crosslinking effect of Ti^{3+}. (c) Dynamic light scattering (DLS) spectra of sols. (d) Photographs showing slowly rotating flasks containing different sols. For control sol, the low viscosity dictates that little liquid remains on the inwall of the flask during rotation, while for target sol, the high viscosity remains a clear liquid membrane. (e) Cyclic voltammetry (CV) results of different substrates.

disadvantageous for the assembly of compact structures. Second, the bulky acetylacetone produces holes during pyrolysis process inevitably. To inhibit the formation of holes and enhance the coverage of TiO_2 film on FTO substrate, on one hand, it is encouraged to reduce moderately the content of acetylacetone-containing precursor by substitution with other reagents. On the other hand, it is desired to provide strong driving forces to promote interparticle cross-linking and assembly. In this work, we explore the modification of conventional sol solution by introducing Ti^{3+}, to modulate crystallization and realize the modification of TiO_2 by self-doping. For further measurement and characterization, the samples without and with Ti^{3+} modification are denoted as Control and Target, respectively. As will be discussed later, the Ti^{3+}/Ti^{4+} molar ratio of 1 results in optimal photovoltaic performances of PSCs, so this ratio is applied for various measurements. More experimental details are available in Supplementary Material.

Control sol exhibits light orange color, while target sample mixing with Ti^{3+} results in a significantly intensified purple color (Fig. 1(b)). According to a check experiment (Fig. S1, Supplementary Material), the color change should be ascribed to acetylacetone, and such an intensified color demonstrates the strong coordination of acetylacetone with Ti^{3+} according to coordination chemistry. It is reasonably inferred that Ti^{3+} can effectively cross-link sol particles by such strong coordination, and the related mechanism is illustrated in Fig. 1(b). The cross-link effect can be evidenced by dynamic light scattering (DLS) measurement. As shown in Fig. 1(c), the average size of control sol particles exhibits a small value of 8.3 nm and a rather narrow size distribution. In comparison, target sol particles swell the average size significantly to 19.0 nm, accompanied by an obvious broadened size distribution. It is also noted that the introduction of Ti^{3+} alters the hydromechanics of sol system. The control sol is a nonelectrolyte with a low viscosity (η) of 5.4 mPa·s, whereas upon addition of ionic Ti^{3+} as the electrolyte, the target sample almost doubles the η value to 10.6 mPa·s. As intuitively shown in Fig. 1(d), the more viscous target sol exhibits a stronger adhesion with glass substrate and shows an obviously better film formation behavior.

In subsequent annealing process, the deposited gel undergoes condensation, pyrolysis and oxidation to form TiO_2 film with rather pure anatase phase (Fig. S2). The coverage and compactness of TiO_2 film dictate the scale of current leakage and thus the performances of PSCs. Therefore, the formation of hole structures should be inhibited. To evaluate the coverage of TiO_2 on FTO substrate, cyclic voltammetry measurement was performed [46]. In this measurement, the substrates as the working electrodes were immersed in aqueous electrolyte of $[Fe(CN)_6]^{3-}/[Fe(CN)_6]^{4-}$. When a forward bias was applied, the oxidation of $[Fe(CN)_6]^{4-}$ occurred at the interfaces of FTO/electrolyte, and oxidation wave was generated. When FTO is covered by TiO_2, since the TiO_2/electrolyte junction is diode-like, the oxidation reaction is blocked. As the scan rate is fast, the intensity of integrated oxidation current is almost proportional to the area of contacted FTO/electrolyte interfaces. As shown in Fig. 1(e), bare FTO substrate exhibits a rather large oxidation peak intensity with a relatively small peak position of 0.92 V. When control TiO_2 layer is constructed, the oxidation peak intensity dramatically declines, and the peak position increases to 0.98 V. This indicates that due to the shield of FTO surface, the oxidation process becomes more difficult with an enhanced overpotential. When target TiO_2 layer is constructed, the intensity of oxidation peak becomes even weaker, and the peak value further increases to 1.24 V. This indicates that compared with control sample, target TiO_2 layer significantly enhances its coverage on FTO surface. As shown in Fig. S3, the annealing of control gel generates a fluffy porous honeycomb-like TiO_2 solid. In stark contrast, the annealing of target gel generates a dense gypsum-like TiO_2 powder. This phenomenon indicates that target TiO_2 film exhibits fewer hole structures. As shown in atomic force microscopy (AFM) images (Fig. S4), target TiO_2 film exhibits a smaller root mean square (RMS) roughness of 0.41 nm than that of control film (0.55 nm). The smooth surface of target TiO_2 should result from less hole and larger surface coverage.

2.2. Facilitated electron extraction based on moderate TiO_2 surface chemistry modulation

Electron transfer from perovskite to ETL is an important factor that dictates device performance [47]. To study electron extraction kinetics, steady state and time resolved photoluminescence spectra (TRPL) of $CsPbI_3$ perovskite on different TiO_2 substrates were recorded. When $CsPbI_3$ perovskite is deposited on TiO_2 substrates, PL intensity and decay behavior on one hand are influenced by electron-hole recombination within perovskite film, on the other hand, should be ascribed to interfacial electron extraction [48]. For conventional thicker perovskite layer, electron-hole recombination within perovskite predominates. When the light beam hits on perovskite surface, it is discovered that different TiO_2 substrates did not influence PL intensity or decay lifetime notably (Fig. S5). This indicates that the quality of $CsPbI_3$ perovskite was not influenced notably by the choice of TiO_2 substrates. If perovskite layer became thinner enough (240 nm, Fig. S6, see Supplementary Material for experimental details), when light beam hits the glass side, more proportion of perovskite approach perovskite/TiO_2 interface, and electron extraction plays a major role. In this case, it is discovered that PL intensity based on target TiO_2 substrate was obviously lower than that of control TiO_2 substrate (Fig. 2(a)), meanwhile target TiO_2 substrate resulted in a shorter decay lifetime (2.66 ns) over control sample (4.13 ns, Fig. 2(b), Table S1). This indicates that target TiO_2 substrate is advantageous for electron extraction.

To probe the causes of improved electron extraction kinetics, the doping effect of target TiO_2 material was investigated initially. As shown in X-ray photoelectron (XPS) spectra, in target TiO_2, Ti 2p peak signal shifts to smaller binding energy with the emergence of Ti^{3+} shoulder peak (Fig. 2(c)) [35]. This indicates the successful doping of Ti^{3+} in target TiO_2. Owing to charge-compensating characteristic, oxygen vacancy should also form, despite that self-doping leads to negligible differences in terms of oxygen in XPS (Fig. S7). Electron paramagnetic resonance (EPR) measurement provides the structural information of TiO_2 samples by testing magnetism. The results demonstrate that control TiO_2 is almost nonmagnetic, while target TiO_2 shows noticeable magnetism (Fig. 2(d)). The magnetism of TiO_2 sample originates from unpaired electrons, and the signal can be further resolved to Ti^{3+}, oxygen vacancy (O_v), and surface adsorbed super-oxygen anion (O_2^-) [49]. The formation of O_v results from charge-compensating characteristic. O_v as the point defect can accumulate electrons and generate magnetic signal [24]. Since Ti^{3+} is uniformly mixed in precursor solution, O_v can distribute both in bulk TiO_2 and on TiO_2 surface. Theoretically, the formation energy of surface O_v is smaller than bulk O_v [22]. Experimentally, the emergence of O_2^- signal proves that O_v successfully form on target TiO_2 surface, because the adsorption of molecular O_2 can only occurs on surface O_v sites, then electron transfer to O_2 occurs, forming O_2^- [50]. In Raman scattering spectra (Fig. S8), the characteristic Ti—O vibrational peak shifts to larger wavenumber with declined intensity. This is due to the formation of oxygen vacancy in TiO_2 skeleton, and low-valent Ti^{3+} dopant results in weaker Ti—O bonds [35].

Based on the self-doping properties, the reasons for enhanced electron extraction dynamics in target TiO_2 are investigated

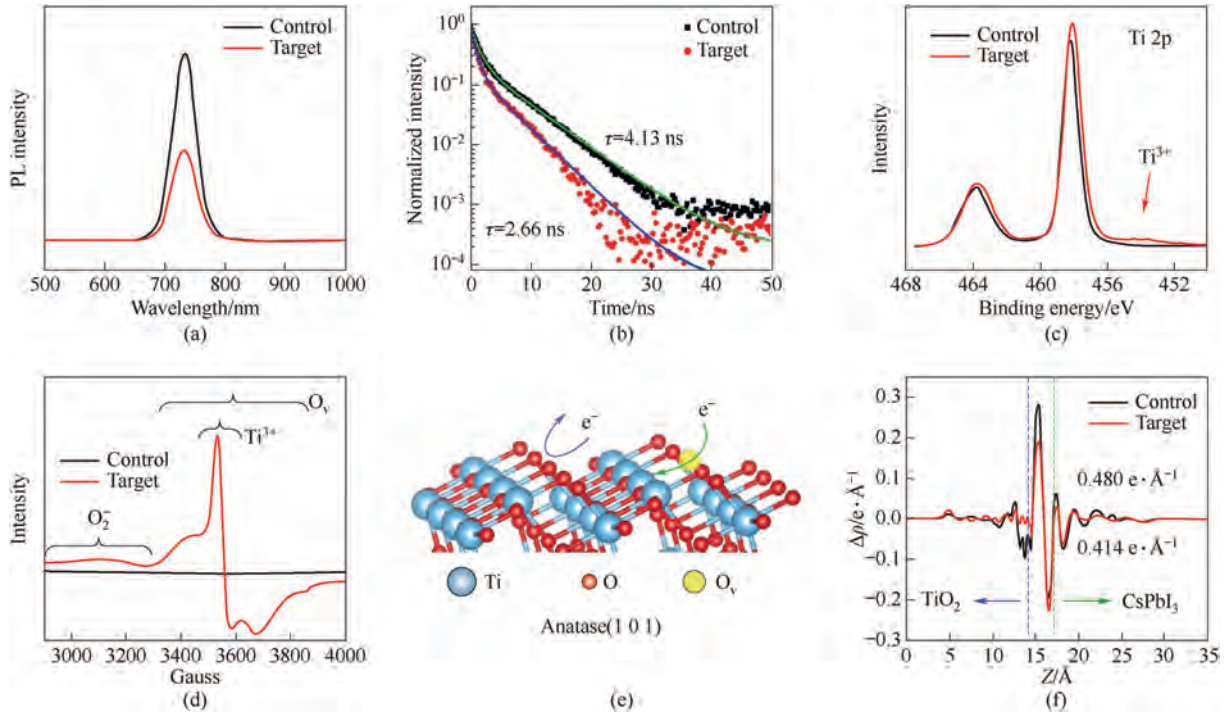

Fig. 2. (a) Steady state PL emission spectra and (b) time-resolved PL decay spectra of thin $CsPbI_3$ perovskite films on different TiO_2 substrates. (c) XPS spectra of Ti. (d) EPR spectra of various TiO_2 samples and determination of magnetically active species. (e) Schematic mechanism showing that moderate surfaced oxygen vacancies on TiO_2 surface can facilitate interfacial electron extraction. (f) Differential charge density diagram of adjacent Ti-Pb cations at $CsPbI_3/TiO_2$ heterojunction interface (1 Å=0.1 nn).

systematically. Interfacial electron extraction on one hand is influenced by electronic coupling, which is influenced by surface chemistry of heterojunction materials on both sides. Photoelectrons transfer from perovskite conduction band to TiO_2 conduction band. Lead and titanium cations contribute the conduction band of perovskite and TiO_2, respectively [1,44]. Therefore, in electron extraction process, surface titanium cations and surface O_v serve as electron acceptors [22]. After extraction, the electron transports within TiO_2 through hopping and finally is collected by glass electrode. Unfortunately, conventional TiO_2 is obtained by annealing in ambient atmosphere with an oxygen-rich surface. Oxygen anions with large electronegativity can screen surface Ti cations and serve as kinetic barriers, resulting in a disadvantageous electron transfer (Fig. 2(e)) [22]. In this sense, it is expected that modulation of TiO_2 surface chemistry to create a moderate oxygen-deficient environment can be beneficial. In contrast, target TiO_2 exposes surface Ti cations by forming surface O_v. O_v acts as electron trapping site to drive electron leave perovskite, then the electrons accumulated at O_v are transferred to adjacent surface Ti cations (Fig. 2(e)) [24]. This is supported by density functional theory (DFT) calculation (details are available in Supplementary Material and schematic electron density diagram of model $CsPbI_3/TiO_2$ heterojunction is shown in Fig. S9). The results indicate that for $CsPbI_3/TiO_2$ heterojunction, surface oxygen anions at anatase (1 0 1) plane obstruct the electrode cloud coupling of Ti^{4+} and Pb^{2+} from perovskite. In this case, differential charge density exhibits a large extremum value ($\Delta\rho$, the difference of maximum and minimum value) of 0.480 e·Å^{-1}, indicating a relatively disadvantageous interfacial electron transfer (Fig. 2(f)). For target TiO_2, when a two-coordinated oxygen vacancy defect (O_v) exists on surface, the differential charge density of adjacent Ti-Pb exhibits a reduced extremum value ($\Delta\rho$) of 0.414 e·Å^{-1}. This indicates that the absence of surface oxygen anions and the removal of surface barrier can enhance interfacial coupling of electron cloud, thus interfacial electron extraction is favored (Fig. 2(f)).

2.3. Advantageous band alignment and electron transport based on TiO_2 self-doping

On the other hand, interfacial electron extraction dynamics can be influenced by energy level alignment. $CsPbI_3$ perovskite exhibits a relatively shallow Fermi energy level ($E_F = -4.00$ eV) [19]. This indicates that when $CsPbI_3$ forms a heterojunction with TiO_2 showing a deeper work function, the conduction band of $CsPbI_3$ can bend upward. Therefore, an interfacial electron transfer barrier is formed, whose height is determined by the E_F difference of two materials [25]. The results of ultraviolet photoelectron spectra (UPS, Fig. S10) and Tauc graph (Fig. S11) were applied to determine band structure of heterojunction, and the results are shown in Fig. 3(a), (b) and Table S2. The results indicate that control TiO_2 exhibits a relatively deep Fermi energy level (E_F) of −4.17 eV. As a result, the conduction band of $CsPbI_3$ bends upward, forming a high interfacial barrier ($E_b = \Delta E_F$) of 0.17 eV. Meanwhile, the conduction band energy level of bulk TiO_2 is higher by 0.06 eV (ΔE_c) than that of $CsPbI_3$ (Fig. 3(a)). This indicates that for control TiO_2, interfacial thermodynamic and kinetic barriers exist simultaneously. In target TiO_2, O_v and Ti^{3+} act as the donor-like defect states. Due to such a self-doping effect, the enhanced n-type semiconductor property and a shallower E_F of −4.12 eV is measured [34,35,51]. In this case, the E_F difference between TiO_2 and $CsPbI_3$ is decreased, and the upward conduction band bending of $CsPbI_3$ is slight. As a result, interfacial barrier (E_b) reduces to 0.12 eV, meanwhile ΔE_c almost disappears (Fig. 3(b)). The results indicate that the moderate shallower E_F of target TiO_2 is advantageous for interfacial electron extraction.

Material conductivity dictates electron transport and collection. The conductivity properties of ETL were tested by space charge limited current (SCLC) measurement [52]. The results are shown in Fig. 3(c), Fig. S12, and Table S2, with theoretical and experimental details available in Supplementary material. The target TiO_2 exhibits a higher trap-filling limit voltage (V_{TFL}) value

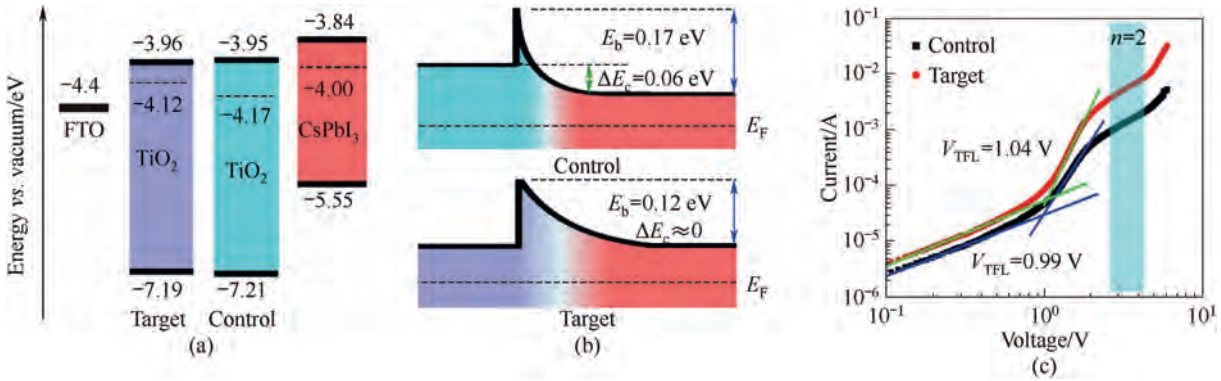

Fig. 3. (a) Diagram of determined band structure $CsPbI_3/TiO_2$ heterojunction. (b) Band bending and interfacial barrier at $CsPbI_3/TiO_2$ heterojunction. (c) SCLC curves based on various TiO_2 samples. The device exhibits the electron-only structure of FTO/TiO_2/carbon. TiO_2 was constructed by 20 spin coating layers to improve the accuracy of layer thickness measurement.

of 1.04 V than the control of 0.99 V. This is indicative of a higher electron density level based on self-doping. Besides, electron transport information can be extracted from the SCLC regime (with the curve slope $n = 2$). The target TiO_2 film exhibits a higher electron mobility and conductivity than control one (electron mobility: 3.66×10^{-4} *vs.* 9.98×10^{-5} $cm^2 \cdot V^{-1}s^{-1}$, conductivity: 2.61×10^{-6} *vs.* 6.26×10^{-7} $S \cdot cm^{-1}$). In TiO_2, Ti^{3+} and oxygen vacancies serve as the medium for electron transport [37,38]. This indicates that moderate self-doping of TiO_2 can promote electron transport.

2.4. Photovoltaic performances of $CsPbI_3$ C-PSCs

HTL-free $CsPbI_3$ C-PSCs with the structure of FTO/TiO_2/$CsPbI_3$/carbon were fabricated, and photovoltaic performances were investigated. Device structure is illustrated in Fig. S13, and the experimental details are available in Supplementary material. As summarized in Fig. 4(a), Table S4 and Fig. S14, control devices exhibit a moderate average PCE of 17.24% (V_{oc} = 1.090 V, J_{sc} = 19.79 mA·cm^{-2}, FF = 79.90%). In comparison, target TiO_2-based devices deliver a higher PCE of 18.16% (V_{oc} = 1.120 V, J_{sc} = 19.82 mA·cm^{-2}, FF = 81.79%). Notably, the champion device delivers a PCE of 18.62% (V_{oc} = 1.132 V, J_{sc} = 19.84 mA·cm^{-2}, FF = 82.92%), representing one of the highest levels in the field of inorganic C-PSCs [39–43]. The *J–V* curves of champion devices are illustrated in Fig. 4(b). The improvement of PCE based on target TiO_2 is mainly contributed by increment of V_{oc} and FF. As discussed above, this should be ascribed to the improved surface morphology with less holes that reduces recombination loss, as well as the facilitated electron extraction dynamics. The influence of the ratio of Ti^{3+}/Ti^{4+} in precursor on photovoltaic parameters was investigated, and the ratio of 1 is optimal (Table S5, Fig. S15). The steady-state power output (SPO) curves at optimal voltages are shown in Fig. 4(c). Both devices could output power at the

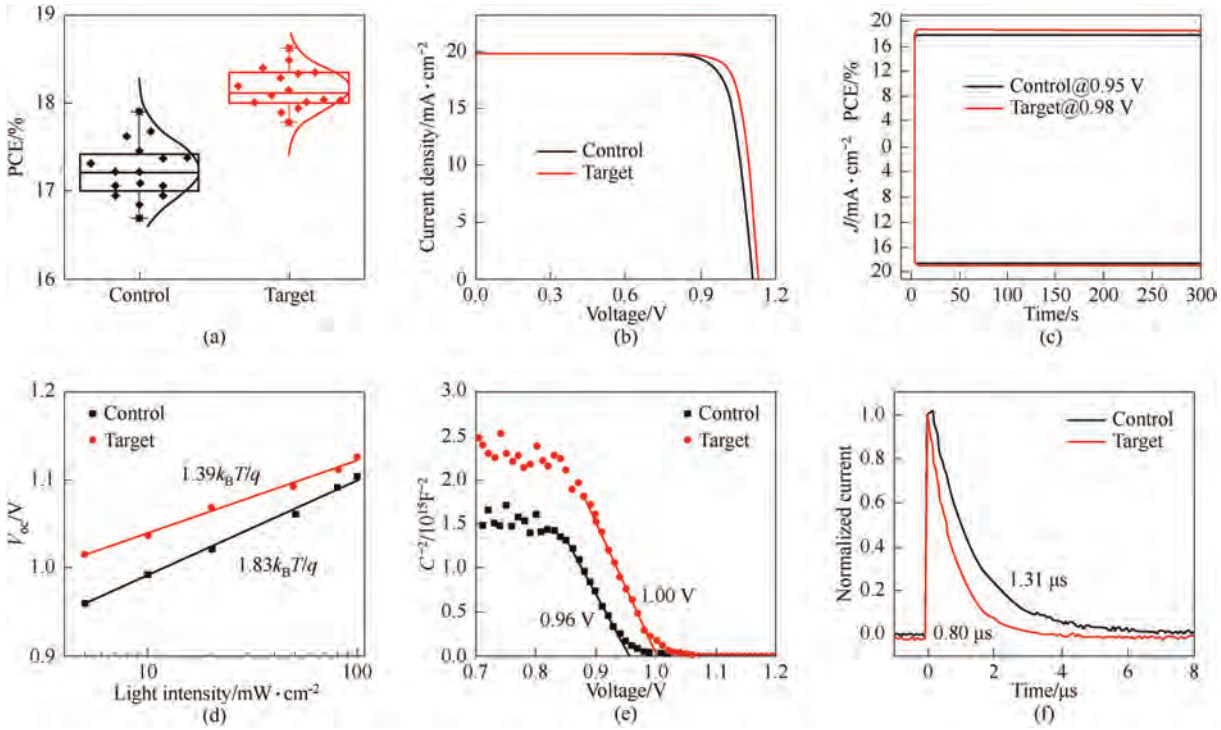

Fig. 4. (a) PCE statistic distribution of C-PSCs including 16 individual devices each. (b) *J–V* curves of champion PSCs. (c) Steady-state power output (SPO) curves of PSCs. (d) V_{oc} dependence on light intensity, (e) Mott-Schottky test, and (f) TPC curves of devices based on different TiO_2 ETL.

maximum power point without notable loss under continuous illumination within 5 min. External quantum efficiency (EQE) curves of the devices are shown in Fig. S16, and the integrated current values match the J_{sc} values in a good way.

The results in electrochemical impedance spectroscopy (EIS, Fig. S17) show that target TiO_2 substrate enhances recombination resistance, indicating that charge recombination loss is inhibited [36]. In light intensity-dependent $J-V$ measurement (Fig. 4(d) and Fig. S18) [53], the fitted smaller ideal factor value based on target TiO_2 (1.39) than the control one (1.83) is indicative of an inhibited trap-assisted recombination under device operating state, and a more efficient V_{oc} output translates to a higher FF level. In Mott-Schottky test (Fig. 4(e)) [54], target TiO_2 resulted in a larger built-in electric field (1.00 V) than the control (0.96 V). This indicates an optimal charge separation driving force. In transient photocurrent (TPC) test (Fig. 4(f)) [13], target TiO_2 resulted in a shorter charge transfer time (0.80 μs) than the control (1.31 μs). This indicates that the photo-generated charges transfer faster in the former case. In transient photovoltage (TPV) test (Fig. S19), target TiO_2 resulted in a slower charge recombination time (7.88 μs) than the control (4.61 μs). This is conductive to the inhibited charge recombination dynamics in the former.

3. Conclusions

In this work, a functional TiO_2 ETL was designed and constructed by a novel Ti^{3+} self-doping strategy in the application of $CsPbI_3$ C-PSCs. The results demonstrate that Ti^{3+} dopant in precursor can effectively facilitate the assembly of titanium sol particles, reduce the content of pore-forming reagent, and enhance the adhesion of precursor to glass substrate. Therefore, a compact TiO_2 ETL film with less hole structure is constructed. Besides, the doped TiO_2 results in a shallower Fermi level and induce the moderate formation of surface oxygen vacancies. As a result, the optimized energy band alignment as well as the stronger interfacial electronic coupling facilitate interfacial electron extraction. The champion device delivers a promising PCE value of 18.62%, representing one of the highest levels in the field of inorganic C-PSCs.

It should be noted that TiO_2 can play multiple roles in electron collection. On the one hand, defects are important for intrinsic electron extraction and transport. On the other hand, defects can also trap electrons and facilitate recombination loss. The rate of recombination is dictated by the concentration and the energy level position of defect states. Therefore, the defects within TiO_2 should be manipulated. In our case, since the overall device efficiency is enhanced, the concentration of introduced defects (oxygen vacancies and Ti^{3+}) has been optimized experimentally, so the benefits surpass the drawbacks. Conventional buried interface engineering strategies often claim the passivation of TiO_2 surface [55]. This can be true due to the interaction of modifiers with defects, yet the outcome of defect passivation should be evaluated. We hypothesize that in buried interface engineering, the bottom surface of perovskite can also be passivated, which seems to be predominant and plays a major role in efficiency enhancement. Therefore, the drawbacks in intrinsic defects of TiO_2 could be overestimated in some cases, and device efficiency can be less sensitive to intrinsic defects within TiO_2, at least to some extent.

CRediT Authorship Contribution Statement

Xin Peng: Formal analysis, Conceptualization, Investigation, Data curation. Rong Huang: Data curation, Formal analysis. Wenran Wang: Data curation, Methodology, Conceptualization, Writing − original draft, Investigation. Jianxin Zhang: Data curation, Formal analysis. Zhenxiao Pan: Funding acquisition. Yueping Fang: Supervision. Huashang Rao: Writing − review & editing, Funding acquisition. Xinhua Zhong: Funding acquisition, Writing − review & editing. Guizhi Zhang: Investigation, Supervision, Formal analysis.

Declaration of Competing Interest

The authors declare the following financial interests/personal relationships which may be considered as potential competing interests: Xinhua Zhong reports financial support was provided by National Natural Science Foundation of China. Xinhua Zhong reports a relationship with National Natural Science Foundation of China that includes: funding grants. If there are other authors, they declare that they have no known competing financial interests or personal relationships that could have appeared to influence the work reported in this paper.

Acknowledgements

This work was supported by the National Natural Science Foundation of China (U21A20310, 22278164, 22122805, and 22308112), the Natural Science Foundation of Guangdong Province, China (2023A1515110634), the Science and Technology Program of Guangzhou, China (2023A04J0665), and China Postdoctoral Science Foundation (2023M741214).

Supplementary Material

Experimental details can be found in the Supplementary Material. Supplementary data to this article can be found online at https://doi.org/10.1016/j.cjche.2025.03.022.

References

[1] A.K. Jena, A. Kulkarni, T. Miyasaka, Halide perovskite photovoltaics: background, status, and future prospects, *Chem. Rev.* 119 (5) (2019) 3036−3103.
[2] H. Chen, C. Liu, J. Xu, A. Maxwell, W. Zhou, Y. Yang, Q.L. Zhou, A.S.R. Bati, H.Y. Wan, Z.W. Wang, L.W. Zeng, J.K. Wang, P. Serles, Y. Liu, S. Teale, Y.J. Liu, M.I. Saidaminov, M.Z. Li, N. Rolston, S. Hoogland, T. Filleter, M.G. Kanatzidis, B. Chen, Z.J. Ning, E.H. Sargent, Improved charge extraction in inverted perovskite solar cells with dual-site-binding ligands, *Science* 384 (6692) (2024) 189−193.
[3] B. Li, D. Gao, S.A. Sheppard, W.D.J. Tremlett, Q. Liu, Z. Li, A.J.P. White, R.K. Brown, X. Sun, J. Gong, S. Li, S. Zhang, X. Wu, D. Zhao, C. Zhang, Y. Wang, X.C. Zeng, Z. Zhu, N.J. Long, Highly efficient and scalable p-i-n perovskite solar cells enabled by poly-metallocene interfaces, *J. Am. Chem. Soc.* 146 (19) (2024) 13391−13398.
[4] W.R. Wang, J.X. Zhang, H.S. Guo, Z.X. Pan, H.S. Rao, G.Z. Zhang, X.H. Zhong, Limitations and progresses in carbon-based cesium lead halide perovskite solar cells, *ChemSusChem* 17 (11) (2024) e202301761.
[5] C. Dong, B.J. Xu, D.M. Liu, E.G. Moloney, F.R. Tan, G.T. Yue, R. Liu, D.Y. Zhang, W.F. Zhang, M.I. Saidaminov, Carbon-based all-inorganic perovskite solar cells: progress, challenges and strategies toward 20% efficiency, *Mater. Today* 50 (2021) 239−258.
[6] H.N. Chen, S.H. Yang, Methods and strategies for achieving high-performance carbon-based perovskite solar cells without hole transport materials, *J. Mater. Chem. A* 7 (26) (2019) 15476−15490.
[7] A.M. Elseman, C.Y. Xu, Y. Yao, M. Elisabeth, L.B. Niu, L. Malavasi, Q.L. Song, Electron transport materials: evolution and case study for high-efficiency perovskite solar cells, *Sol. RRL* 4 (7) (2020) 2000136.
[8] Y. Zhou, X. Li, H. Lin, To be higher and stronger: metal oxide electron transport materials for perovskite solar cells, *Small* 16 (15) (2020) 1902579.
[9] Y. Bai, I. Mora-Seró, F. De Angelis, J. Bisquert, P. Wang, Titanium dioxide nanomaterials for photovoltaic applications, *Chem. Rev.* 114 (19) (2014) 10095−10130.
[10] Y. Wang, M.I. Dar, L.K. Ono, T. Zhang, M. Kan, Y. Li, L. Zhang, X. Wang, Y. Yang, X. Gao, Y. Qi, M. Grätzel, Y. Zhao, Thermodynamically stabilized β-$CsPbI_3$-based perovskite solar cells with efficiencies >18%, *Science* 365 (2019) 591−595.
[11] Y.Q. Cui, J.J. Shi, F.Q. Meng, B.C. Yu, S. Tan, S. He, C.Y. Tan, Y.M. Li, H.J. Wu, Y.H. Luo, D.M. Li, Q.B. Meng, A versatile molten-salt induction strategy to achieve efficient $CsPbI_3$ perovskite solar cells with a high open-circuit voltage >1.2 V, *Adv. Mater.* 34 (45) (2022) e2205028.

[12] S. Tan, B.C. Yu, Y.Q. Cui, F.Q. Meng, C.J. Huang, Y.M. Li, Z.J. Chen, H.J. Wu, J.J. Shi, Y.H. Luo, D.M. Li, Q.B. Meng, Temperature-reliable low-dimensional perovskites passivated black-phase $CsPbI_3$ toward stable and efficient photovoltaics, *Angew. Chem., Int. Ed.* 61 (23) (2022) e202201300.
[13] S. Tan, C.Y. Tan, Y.Q. Cui, B.C. Yu, Y.M. Li, H.J. Wu, J.J. Shi, Y.H. Luo, D.M. Li, Q.B. Meng, Constructing an interfacial gradient heterostructure enables efficient $CsPbI_3$ perovskite solar cells and printed minimodules, *Adv. Mater.* 35 (28) (2023) e2301879.
[14] Y.W. Duan, J.G. Wang, D.F. Xu, P.G. Ji, H. Zhou, Y. Li, S.M. Yang, Z. Xie, X.H. Hai, X.R. Lei, R. Sun, Z.H. Fan, K. Zhang, S.Z. Liu, Z.K. Liu, 21.41%-efficiency $CsPbI_3$ perovskite solar cells enabled by an effective redox strategy with 4-fluorobenzothiohydrazide in precursor solution, *Adv. Funct. Mater.* 34 (10) (2024) 2312638.
[15] J.M. Qiu, X.Y. Mei, M.X. Zhang, G.L. Wang, S.W. Zou, L. Wen, J.M. Huang, Y. Hua, X.L. Zhang, Dipolar chemical bridge induced $CsPbI_3$ perovskite solar cells with 21.86% efficiency, *Angew. Chem., Int. Ed.* 63 (18) (2024) e202401751.
[16] J.X. Zhang, G.Z. Zhang, P.Y. Su, R. Huang, J.G. Lin, W.R. Wang, Z.X. Pan, H.S. Rao, X.H. Zhong, 1D choline-PbI_3-based heterostructure boosts efficiency and stability of $CsPbI_3$ perovskite solar cells, *Angew. Chem., Int. Ed.* 62 (25) (2023) e202303486.
[17] W.R. Wang, X. Peng, J.X. Zhang, J.G. Lin, R. Huang, G.Z. Zhang, H.S. Guo, Z.X. Pan, X.H. Zhong, H.S. Rao, Dimethylamine oxalate manipulating CsPbI3 perovskite film crystallization process for high efficiency carbon electrode based perovskite solar cells, *J. Energy Chem.* 93 (2024) 221−228.
[18] Q.X. Zhang, H.C. Liu, X.Z. Wei, Y.F. Song, C.Y. Lv, W.P. Li, L.Q. Zhu, Y.S. Lan, Y.J. Du, K.X. Wang, P.G. Yin, C.Q. Lin, Z.D. Lin, Y. Bai, Q. Chen, S.H. Yang, H.N. Chen, Deploying a dipole electric field at the $CsPbI_3$ perovskite/carbon interface for enhancing hole extraction and photovoltaic performance, *Small* 20 (40) (2024) 2402061.
[19] J.G. Lin, R. Huang, X. Peng, J.X. Zhang, G.Z. Zhang, W.R. Wang, Z.X. Pan, H.S. Rao, X.H. Zhong, Eliminating hole extraction barrier in 1D/3D perovskite heterojunction for efficient and stable carbon-based $CsPbI_3$ solar cells with a record efficiency, *Adv. Mater.* 36 (33) (2024) e2404561.
[20] D.M. Hausmann, R.G. Gordon, Surface morphology and crystallinity control in the atomic layer deposition (ALD) of hafnium and zirconium oxide thin films, *J. Cryst. Growth* 249 (1−2) (2003) 251−261.
[21] T.S. Sherkar, C. Momblona, L. Gil-Escrig, J. Ávila, M. Sessolo, H.J. Bolink, L. Jan Anton Koster, Recombination in perovskite solar cells: significance of grain boundaries, interface traps, and defect ions, *ACS Energy Lett.* 2 (5) (2017) 1214−1222.
[22] W.B. Jiang, H. Loh, B.Q.L. Low, H.J. Zhu, J. Low, J.Z.X. Heng, K.Y. Tang, Z.B. Li, X. J. Loh, E.Y. Ye, Y.J. Xiong, Role of oxygen vacancy in metal oxides for photocatalytic CO_2 reduction, *Appl. Catal. B Environ.* 321 (2023) 122079.
[23] W.P. Hu, S.F. Yang, S.H. Yang, Surface modification of TiO_2 for perovskite solar cells, *Trends Chem.* 2 (2) (2020) 148−162.
[24] Z.L. Wang, R.J. Lin, Y.N. Huo, H.X. Li, L.Z. Wang, Formation, detection, and function of oxygen vacancy in metal oxides for solar energy conversion, *Adv. Funct. Mater.* 32 (7) (2022) 2109503.
[25] E. Liu, B. Zhu, J. Luo, The Physics of Semiconductors, seventh ed., Publishing House of Electronic Industry, Beijing, 2017.
[26] H. Zheng, C.H. Wang, X.T. Zhang, Y.Y. Li, H. Ma, Y.C. Liu, Control over energy level match in keggin polyoxometallate-TiO_2 microspheres for multielectron photocatalytic reactions, *Appl. Catal. B Environ.* 234 (2018) 79−89.
[27] H.Y. Zhang, J.J. Shi, X. Xu, L.F. Zhu, Y.H. Luo, D.M. Li, Q.B. Meng, Mg-doped TiO_2boosts the efficiency of planar perovskite solar cells to exceed 19%, *J. Mater. Chem. A* 4 (40) (2016) 15383−15389.
[28] M.H. Lv, W. Lv, X. Fang, P. Sun, B.C. Lin, S. Zhang, X.Q. Xu, J.N. Ding, N.Y. Yuan, Performance enhancement of perovskite solar cells with a modified TiO_2 electron transport layer using Zn-based additives, *RSC Adv.* 6 (41) (2016) 35044−35050.
[29] T.T. Wu, C. Zhen, H.Z. Zhu, J.B. Wu, C.X. Jia, L.Z. Wang, G. Liu, N.G. Park, H.M. Cheng, Gradient Sn-doped heteroepitaxial film of faceted rutile TiO_2 as an electron selective layer for efficient perovskite solar cells, *ACS Appl. Mater. Interfaces* 11 (21) (2019) 19638−19646.
[30] H.P. Zhou, Q. Chen, G. Li, S. Luo, T.B. Song, H.S. Duan, Z.R. Hong, J.B. You, Y.S. Liu, Y. Yang, Photovoltaics. Interface engineering of highly efficient perovskite solar cells, *Science* 345 (6196) (2014) 542−546.
[31] B.X. Chen, H.S. Rao, W.G. Li, Y.F. Xu, H.Y. Chen, D.B. Kuang, C.Y. Su, Achieving high-performance planar perovskite solar cell with Nb-doped TiO_2 compact layer by enhanced electron injection and efficient charge extraction, *J. Mater. Chem. A* 4 (15) (2016) 5647−5653.
[32] J. Peng, F. Kremer, D. Walter, Y. Wu, Y. Ji, J. Xiang, W. Liu, T. Duong, H. Shen, T. Lu, F. Brink, D. Zhong, L. Li, O. Lee Cheong Lem, Y. Liu, K.J. Weber, T.P. White, K.R. Catchpole, Centimetre-scale perovskite solar cells with fill factors of more than 86 percent, *Nature* 601 (7894) (2022) 573−578.
[33] D.S. Che Halin, A.W. Azhari, M.A.A. Mohd Salleh, N.I. Muhammad Nadzri, P. Vizureanu, M.M. Al Bakri Abdullah, J.A. Wahab, A.V. Sandu, Metal-doped TiO_2 thin film as an electron transfer layer for perovskite solar cells: a review, *Coatings* 13 (1) (2023) 4.
[34] B. Roose, S. Pathak, U. Steiner, Doping of TiO_2 for sensitized solar cells, *Chem. Soc. Rev.* 44 (22) (2015) 8326−8349.
[35] L. Liu, X.B. Chen, Titanium dioxide nanomaterials: self-structural modifications, *Chem. Rev.* 114 (19) (2014) 9890−9918.
[36] W.R. Wang, Y. Lin, G.Z. Zhang, C.T. Kang, Z.X. Pan, X.H. Zhong, H.S. Rao, Modification of compact TiO_2 layer by $TiCl_4$-$TiCl_3$ mixture treatment and construction of high-efficiency carbon-based $CsPbI_2Br$ perovskite solar cells, *J. Energy Chem.* 63 (2021) 442−451.
[37] D. Bing Wang, D. Meng Zhang, D. Xun Cui, Z.W. Wang, M. Rager, P. Yingkui Yang, P. Zhigang Zou, P. Zhong Lin Wang, P. Zhiqun Lin, Unconventional route to oxygen-vacancy-enabled highly efficient electron extraction and transport in perovskite solar cells, *Angew. Chem. Int. Ed.* 59 (4) (2020) 1611−1618.
[38] J.L. Liu, S. Li, Z.X. Qiu, Y. Liu, C. Qiu, W.H. Zhang, J.H. Qi, K. Chen, W. Wang, C.Y. Wang, Z.Z. Cui, Y.Q. Su, Y. Hu, A.Y. Mei, H.W. Han, Stratified oxygen vacancies enhance the performance of mesoporous TiO_2 electron transport layer in printable perovskite solar cells, *Small* 19 (32) (2023) e2300737.
[39] G.Z. Zhang, J.X. Zhang, Z.C. Yang, Z.X. Pan, H.S. Rao, X.H. Zhong, Role of moisture and oxygen in defect management and orderly oxidation boosting carbon-based $CsPbI_2$ Br solar cells to a new record efficiency, *Adv. Mater.* 34 (40) (2022) e2206222.
[40] Y.Y. Liao, J.X. Zhang, W.R. Wang, Z.C. Yang, R. Huang, J.G. Lin, L. Che, G.Y. Yang, Z.X. Pan, H.S. Rao, X.H. Zhong, Anti-dissociation passivation *via* bidentate anchoring for efficient carbon-based $CsPbI_2{\cdot}6Br_{0.4}$ solar cells, *Adv. Funct. Mater.* 33 (20) (2023) 2214784.
[41] H.L. Wang, Y.F. Song, Z.D. Lin, W.P. Li, H.C. Liu, X.Z. Wei, Q.X. Zhang, C.Y. Lv, L. Q. Zhu, K.X. Wang, Y.S. Lan, L. Wang, C.Q. Lin, P.G. Yin, T.L. Song, Y. Bai, Q. Chen, S.H. Yang, H.N. Chen, *In situ* growth of a robust 1D capping layer for stable and efficient CsPbI3 perovskite solar cells without hole transporter, *Adv. Energy Mater.* 14 (16) (2024) 2304038.
[42] J. Wang, Y. Che, Y. Duan, Z. Liu, S. Yang, D. Xu, Z. Fang, X. Lei, Y. Li, S.F. Liu, 21.15%-efficiency and stable γ-$CsPbI_3$ perovskite solar cells enabled by an acyloin ligand, *Adv. Mater.* 35 (12) (2023) e2210223.
[43] Y.Q. Li, X.Y. Lu, Y.T. Mei, C. Dong, D.T. Gangadharan, K. Liu, Z.J. Wang, S.C. Qu, M.I. Saidaminov, W.F. Zhang, F.R. Tan, Blade-coated carbon electrode perovskite solar cells to exceed 20% efficiency through protective buffer layers, *Adv. Funct. Mater.* 33 (34) (2023) 2301920.
[44] X.B. Chen, S.S. Mao, Titanium dioxide nanomaterials: synthesis, properties, modifications, and applications, *Chem. Rev.* 107 (7) (2007) 2891−2959.
[45] M. Cargnello, T.R. Gordon, C.B. Murray, Solution-phase synthesis of titanium dioxide nanoparticles and nanocrystals, *Chem. Rev.* 114 (19) (2014) 9319−9345.
[46] L. Kavan, L. Steier, M. Grätzel, Ultrathin buffer layers of SnO_2 by atomic layer deposition: perfect blocking function and thermal stability, *J. Phys. Chem. C* 121 (1) (2017) 342−350.
[47] Y.H. Li, H.B. Xie, E.L. Lim, A. Hagfeldt, D.Q. Bi, Recent progress of critical interface engineering for highly efficient and stable perovskite solar cells, *Adv. Energy Mater.* 12 (5) (2022) 2102730.
[48] D.W. DeQuilettes, J.J. Yoo, R. Brenes, F.U. Kosasih, M. Laitz, B.D. Dou, D.J. Graham, K. Ho, Y.W. Shi, S.S. Shin, C. Ducati, M.G. Bawendi, V. Bulović, Reduced recombination *via* tunable surface fields in perovskite thin films, *Nat. Energy* 9 (2024) 457−466.
[49] H. Liu, H.T. Ma, X.Z. Li, W.Z. Li, M. Wu, X.H. Bao, The enhancement of TiO_2 photocatalytic activity by hydrogen thermal treatment, *Chemosphere* 50 (1) (2003) 39−46.
[50] K. Komaguchi, T. Maruoka, H. Nakano, I. Imae, Y. Ooyama, Y. Harima, Electron-transfer reaction of oxygen species on TiO_2 nanoparticles induced by sub-band-gap illumination, *J. Phys. Chem. C* 114 (2) (2010) 1240−1245.
[51] M.T. Greiner, L. Chai, M.G. Helander, W.M. Tang, Z.H. Lu, Transition metal oxide work functions: the influence of cation oxidation state and oxygen vacancies, *Adv. Funct. Mater.* 22 (21) (2012) 4557−4568.
[52] Z.J. Wu, Y. Wang, L.C. Li, R.K. Zhang, J. Hong, R. Huang, L. Che, G.Y. Yang, H.S. Rao, Z.X. Pan, X.H. Zhong, Improving the electron transport performance of TiO_2 film by regulating $TiCl_4$ post-treatment for high-efficiency carbon-based perovskite solar cells, *Small* 19 (29) (2023) e2300690.
[53] A.K. Kyaw, D.H. Wang, V. Gupta, W.L. Leong, L. Ke, G.C. Bazan, A.J. Heeger, Intensity dependence of current-voltage characteristics and recombination in high-efficiency solution-processed small-molecule solar cells, *ACS Nano* 7 (5) (2013) 4569−4577.
[54] Z. Yao, Z. Xu, W.G. Zhao, J.R. Zhang, H. Bian, Y.K. Fang, Y. Yang, S.Z. Liu, Enhanced efficiency of inorganic $CsPbI_{3-x}Br_x$ perovskite solar cell *via* self-regulation of antisite defects *Adv*, *Energy Mater* 11 (23) (2021) 2100403.
[55] Z.W. Gao, Y. Wang, W.C.H. Choy, Buried interface modification in perovskite solar cells: a materials perspective, *Adv. Energy Mater.* 12 (20) (2022) 2104030.